

Interaction of diamond mine waste and surface water in the Canadian Arctic

H.A. Rollo¹, H.E. Jamieson^{*}

Queen's University, Department of Geological Sciences and Geological Engineering, Kingston, Canada K7L 3N6

Received 12 August 2005; accepted 27 May 2006

Editorial handling by R. Fuge

Available online 10 August 2006

Abstract

Factors controlling the chemical composition of water interacting with finely-crushed kimberlite have been investigated by sampling pore waters from processed kimberlite fines stored in a containment facility. Discharge water from the diamond recovery plant and surface water from the containment facility, which acts as plant intake water, were also sampled. All waters sampled are pH-neutral, enriched in SO₄, Mg, Ca, and K, and low in Fe. Pore-water samples, representing the most concentrated waters, are characterized by the highest SO₄ (up to 4080 mg l⁻¹), Mg (up to 870 mg l⁻¹), and Ca (up to 473 mg l⁻¹). The water discharged from the processing plant has higher concentrations of all major dissolved constituents than the intake water. The dominant minerals present in the processed fines and the kimberlite ore are serpentine and olivine, with small amounts of Ca sulphate and Fe sulphide restricted to mud xenoclasts. Reaction and inverse modeling suggest that much of the water-rock interaction takes place within the plant and involves the dissolution of chrysotile and Ca sulphate, and precipitation of silica and Mg carbonate. Evapoconcentration also appears to be a significant process affecting pore water composition in the containment facility. The reaction proposed to be occurring during ore processing involves the dissolution of CO_{2(g)} and may represent an opportunity to sequester atmospheric CO₂ through mineral carbonation. © 2006 Elsevier Ltd. All rights reserved.

1. Introduction

The environmental consequences of mining and processing kimberlite ore for the production of diamonds has been a relatively unstudied subject. In particular, the impact of the discharge and storage

of finely crushed kimberlite slurry on the quality of surface water in an arctic environment is unknown. In Canada, economic diamond deposits were first discovered in the Northwest Territories in 1991. By 2003, two mines were operating and producing approximately 15% of the world's diamonds by value (Law-West, 2003). The diamonds are extracted from kimberlite pipes made of heterogeneous rock composed largely of Mg silicate minerals but commonly containing xenoliths and xenoclasts of other material, including mantle-derived minerals as well as sediments incorporated

^{*} Corresponding author. Tel.: +1 6135336181; fax: +1 6135336592.

E-mail address: jamieson@geol.queensu.ca (H.E. Jamieson).

¹ Present address: Lorax Environmental Services, Vancouver, BC.

during intrusion. At the EKATI diamond mine, where this research was conducted, the fine fraction of the processed kimberlite waste is stored in a containment facility created from two modified lake basins. The water in the containment facility is isolated from downstream surface waters by an impermeable dam and only released if water quality criteria are met. The natural surface waters in the area are characterized by very low dissolved solid content and little buffering capacity. The research described in this paper was conducted to determine the chemical consequences of combining crushed kimberlite and nearly pristine water. The objectives were to chemically and mineralogically describe the water-rock system and to elucidate the processes that were controlling the composition of water in the containment facility.

2. EKATI diamond mine

EKATI opened in late 1998 as the first commercial diamond mine to operate in Canada. It is located approximately 300 km NE of the city of Yellowknife (Fig. 1) and approximately 200 km south of the Arctic Circle. This location is above the tree line and within the zone of continuous permafrost in Canada's Arctic, where the climate is

cold (mean annual temperature of -11.8°C) and dry (mean annual precipitation of 250–300 mm; mean open-water evaporation of 200–350 mm, Rescan Environmental Services Inc., 1996).

The mine is situated in the Archean granite-greenstone terrain of the Slave Structural Province of the Canadian Shield. More than 150 kimberlites occur on the property, most in the form of small pipes with surface areas less than 5 ha, and a significant number of these pipes are of economic importance. The kimberlites range in age from 45.2 ± 0.8 to 74.7 ± 6.8 Ma (Nowicki et al., 2003; based on Rb-Sr and U-Pb dating).

The processed kimberlite studied as part of this investigation was derived from the top portion of the Panda kimberlite, the first pipe to be mined at EKATI. The host rock of the Panda kimberlite is a white to grey, medium to coarse-grained, weakly foliated to massive biotite granodiorite with an average composition of 40% quartz, 45% feldspar and 15% biotite (Kjarsgaard et al., 2002; Rescan Environmental Services Inc., 1996). The Panda kimberlite, like all kimberlites at EKATI, originally occupied the bottom of a small lake. This lake was drained and the overlying 15 m to 25 m of glacial and lacustrine sediments were stripped prior to mining. The original pre-mining surface area of the

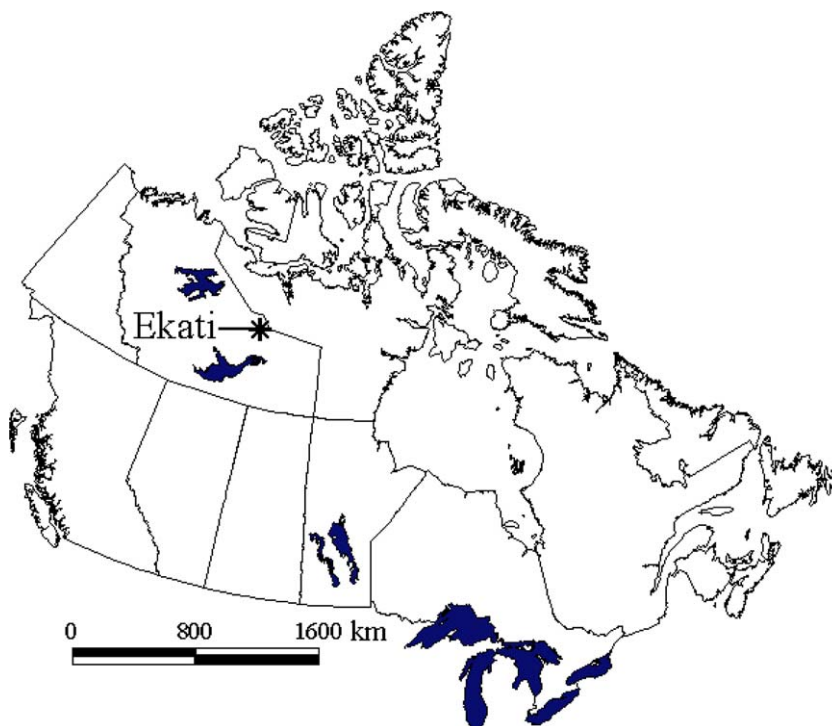


Fig. 1. Map of Canada showing the location of the EKATI mine.

Panda pipe was approximately 3.1 hectares (Carlson et al., 1998).

Like many kimberlites of the Lac de Gras area, the Panda kimberlite is dominated by bedded, volcanoclastic kimberlite, which was probably resedimented back into the crater after eruption (Carlson et al., 1998). This material consists predominantly of olivine macrocrysts, mudstone, and granodiorite xenoliths in a dark, fine-grained matrix composed of serpentine, carbonate and clay minerals. Xenocrysts of garnet, chrome diopside, chromite, as well as fossils, including wood fragments, are common throughout the pipe (Carlson et al., 1998; Nowicki et al., 2003).

The extraction of diamonds from the kimberlite ore involves crushing, washing, sorting, and identification of diamonds using X-ray fluorescence. Approximately 13,000–16,000 wet tonnes of kimberlite ore are processed daily at EKATI (Day et al., 2003). Water for the processing circuit is pumped from a water-reclaim barge located within the processed kimberlite containment facility. Within the processing plant, kimberlite that has previously been crushed to particles <75 mm is conveyed through a circuit where the ore is further crushed, washed, and ultimately sorted into two size fractions: (1) <1 mm; and (2) approximately 1–25 mm. The <1 mm fraction, known as processed kimberlite fines, is sent to a thickening tank to help facilitate dewatering of the fines and recovery of process water. This fine fraction comprises approximately 70% of the total processed kimberlite, and is analogous to mill tailings produced from base and precious metal mines.

Once the processed kimberlite fines have been thickened to a solids content of approximately 45% by weight, they are hydraulically pumped from the process plant to the processed kimberlite fines containment facility, known as the Long Lake Containment Facility (LLCF). To assist in the settling of fine particles from the process water, a coagulant and flocculant are added to the processed kimberlite fines slurry before it enters the thickening tank. The dose of coagulant (PERCOL 368) and flocculant (PERCOL E-10) added to the Panda fines slurry is approximately 35 g and 120 g per tonne of ore processed, respectively (EBA Engineering Consultants Ltd., 1998). These are the only two chemicals added to the processed kimberlite fines.

As shown in Fig. 2, the LLCF is an engineered former lake basin located approximately 3 km west of the process plant. The LLCF has been divided

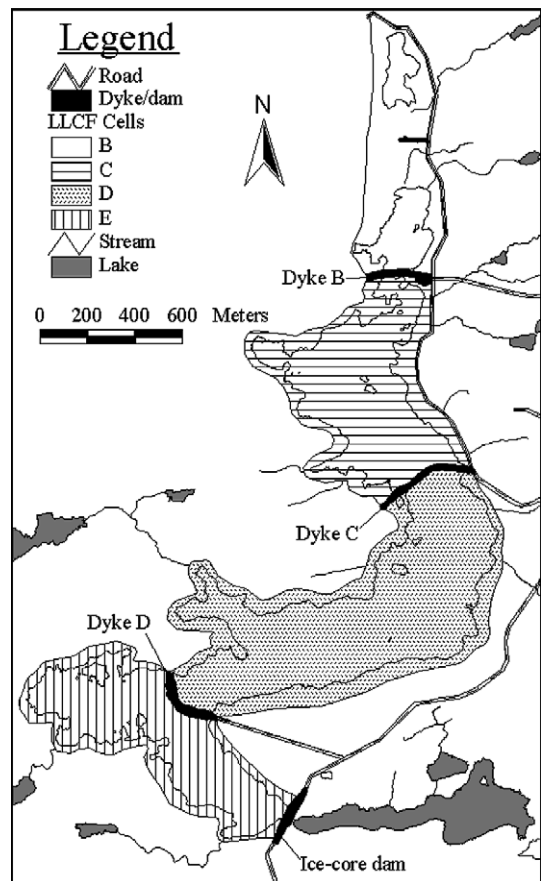


Fig. 2. Long Lake Containment Facility (LLCF). Shaded regions represent the approximate maximum extent of each cell when filled with processed kimberlite fines.

into 4 cells (B, C, D, and E), each separated by filter dykes composed of granite waste rock and glacial till, which have been designed to help control turbidity in the LLCF discharge released to the receiving environment. An ice-core dam at the outlet of the containment facility isolates the LLCF water from the natural drainage of the region. Generally, kimberlite waste is deposited in the LLCF from north to south so that the oldest material (from 1998) is found in the northernmost portion of Cell B. Drilling conducted in March 2001 revealed that the northern portion of Cell B has developed a stratigraphy comprised of three distinct units (Rollo, 2003). The upper layer extends to approximately 1 m below the surface and is characterized by dense, ice-bonded kimberlite fines with a distinctive lack of visible ice layers or lenses. This represents the active layer that develops during the warm summer months. There are no ice lenses or layers in this unit because, as the active layer develops in the summer,

any ice that was present melts and drains from the fines. All pore-water samples reported in this study have been collected from this layer during the summer season when the active layer has thawed. The second layer extends from 1 m to approximately 5 m below the surface of the fines. This zone is typified by cm-scale rhythmic layering of kimberlite fines and ice, thought to represent winter deposition within the LLCF. The third unit extends from approximately 5 m depth to the bottom of the containment facility and is composed of completely saturated unfrozen processed kimberlite fines (Rollo, 2003).

3. Previous work

Prior to the commencement of mining operations in August 1998, unprocessed and simulated processed kimberlite was geochemically characterized (Norecol Dames and Moore, 1997). Both static and kinetic testing were conducted to help determine acid generation potential (AP) and neutralization potential (NP) of the rock types, as well as to determine metal leaching rates in an effort to model discharge from the LLCF.

Static testing, using the Sobek ABA procedures (Sobek et al., 1978), indicates that Panda kimberlite has a high mean NP (240 kg CaCO₃/t) and a relatively low AP (13 kg CaCO₃/t), suggesting that there is no potential for the generation of acidic drainage from unprocessed Panda kimberlite (NPR = 18, where NPR is net potential ratio). Simulated tailings were also produced using Panda kimberlite and subjected to static testing. As was the case for the unprocessed kimberlite ore, static test results from the simulated processed kimberlite fines from the Panda kimberlite indicate a high NP (490.6 kg CaCO₃/t) and a relatively low AP (9.7 kg CaCO₃/t), suggesting that there is no potential for the generation of acidic drainage from processed Panda kimberlite (NPR = 51).

As well as static testing, column tests were used to simulate the conditions that would exist along a flow path through the LLCF. Testing was conducted using 4 simulated tailings samples, including Panda kimberlite, and involved filling a plastic column with approximately 2 kg of sample and then re-circulating cold (~3 °C), de-ionized water through the column at a rate of 2 l/week for several weeks. Results from these tests indicate that dissolution of Panda tailings produces constant pH values (between 7 and 8) and metal release rates that are

initially rapid, and then become erratic with relatively low concentrations having no apparent increasing or decreasing trends (Norecol Dames and Moore, 1997). In addition, the slow dissolution of silicate minerals was predicted to be the dominant weathering mechanism in kimberlite material.

Day et al. (2003) conducted an investigation on the geochemical characteristics of coarse kimberlite reject material stored in a subaerial pile adjacent to the LLCF, as well as the composition of pore and seep water found issuing from this storage pile. This study found that the coarse reject material has high NP values of 78–337 kg CaCO₃/t. The water sampled was relatively high in total dissolved solids, including SO₄, Mg and, in some cases, Fe, which the authors interpret to be the result of low annual precipitation, minor sulphide oxidation coupled with neutralization by Mg silicates, possibly magnified by freeze concentration.

The geochemical reactivity of kimberlite material from the Diavik Diamonds Project, located immediately south of EKATI within the Lac de Gras kimberlite field, was investigated by Baker et al. (2003). Laboratory-based acid–base accounting and humidity cell tests were used to determine the potential behaviour of processed kimberlite waste from Diavik when stored in a surficial impoundment. Their research indicates that, similar to Panda, the Diavik pipe is predominantly pyroclastic kimberlite composed of serpentine and olivine and that weathering of this material in a surface impoundment will produce an effluent with a pH near 8.

While the studies mentioned previously are the only two other investigations of water–rock interactions of Lac de Gras kimberlite materials, studies from other kimberlite bodies have yielded results similar to those observed in the Lac de Gras kimberlite investigations. Borisov et al. (1995) investigated the water issuing from diamond quarries in East Siberia and noted pH values of approximately eight as well as total dissolved solid concentrations approaching 4 to 8 g/l. These waters were dominated by SO₄, Cl, Mg and Ca. Sader et al. (2003) sampled groundwater from exploration drillholes at 5 kimberlite sites in Northeastern Ontario and found high pH values (typically 8–12), as well as high Na, K, Mg, Ca, and SO₄ concentrations. Researchers investigating the controls on spring waters issuing from ultramafic bodies dominated by olivine and serpentine have found Mg- and HCO₃-dominated solutions (Barnes and LaMarche, 1969; Barnes et al., 1967, 1978; Bruni et al., 2002; Pfeifer, 1977). These

studies suggest that the water compositions observed were a result of the open system dissolution of serpentinites in meteoric waters (Bruni et al., 2002).

4. Sampling

4.1. Water

Water samples were collected each summer from 2000 to 2002, and included: (1) processed kimberlite pore-water (60 samples); (2) process plant discharge water (9 samples); and (3) surface water from the LLCF (18 samples). Processed kimberlite fines pore water was collected from the active (seasonally unfrozen) layer of the processed fines located in the northern portion of Cell B (Fig. 2). These samples were acquired using suction lysimeters, which were installed within the unsaturated zone approximately 10 to 20 cm above the water table or the frost table, whichever was closer to the surface. Each lysimeter was purged 3 times prior to analytical sampling. Process plant water was collected from the discharge spigot delivering fines and process water to the containment facility. Surface water samples were collected from the upstream side of Dyke B and Dyke C, respectively (9 samples each), with Dyke C water samples collected from the end of the water-reclaim barge that pumps water to the process plant to be used in the washing of crushed kimberlite ore.

All water samples were prepared in the same manner. Each water sample was vacuum filtered with a 0.45 μm cellulose acetate bottle top filter and a hand pump. The aliquot destined for cation analysis was preserved with high purity trace-element grade (15.9 M) HNO_3 , the aliquot used for anion analysis was left unpreserved and filled to capacity in order to minimize headspace, and the DOC aliquot was preserved with high purity concentrated H_2SO_4 and stored in an amber glass bottle. All samples were stored at 4 °C. In addition, pH, conductivity, temperature, and alkalinity were measured in the field at the time of collection. Attempts to evaluate the redox state of the water were limited by the fact that the waters were clearly in redox disequilibrium as shown by the presence of relatively high DOC (probably related to the wood fragments present in the kimberlite) and high dissolved O_2 (Table 1) (Langmuir, 1996). The waters were analyzed for a wide range of cations by ICP-MS and for anions by ion chromatography (Table 1).

A comprehensive QA/QC program, including field blanks, field duplicates, travel blanks, analyti-

cal replicates, and certified reference materials, was instituted in order to evaluate the quality of data obtained from the water sampling program. These data do not indicate any significant contamination or analytical issues with the LLCF water data. Any water sample with a calculated charge imbalance greater than $\pm 15\%$ was not included in subsequent analysis.

4.2. Solids

Two types of solid samples were collected for this investigation: (1) unprocessed Panda kimberlite; and, (2) processed kimberlite fines. Four Panda kimberlite samples were collected in July 2000 from recently blasted material in the open pit. In addition, 20 samples were collected from drill core obtained from a 1995 exploration drilling program. These drill holes were selected due to the fact that they were oriented sub-horizontally across the top portions of the Panda pipe. Therefore, these samples were assumed to be representative of the ore that was mined, processed, and deposited in the northern portion of Cell B in late 1998. In addition, 27 samples of the processed kimberlite fines were selected from cores that were collected immediately adjacent to each pore water sampling site. These core samples were collected by pushing, or hammering, a length of 5 cm inside diameter PVC pipe into the fines until the frost table was reached. A rubber stopper was then placed in the top of the pipe to help create a partial vacuum as the core sample was removed. Core samples were frozen within 1 h of collection to help arrest any further reaction.

Eighteen polished thin sections of kimberlite ore and 27 sections of processed kimberlite fines were prepared using cool-curing epoxy and no water to ensure that soluble and reactive phases were not altered. An ARL-SEMQ electron microprobe equipped with an EDS (energy dispersive) spectrometer was used to investigate the identity and composition of minerals present within the samples. Standard analytical conditions were used in the collection of data, including an accelerating voltage of 15 kV, a take-off angle of 52.5°, an emission current of 100 mA, a beam current of 40 nA, and a collection time of 200 s.

Sulphide and SO_4 concentrations were determined using direct combustion and BaSO_4 gravimetry, respectively (Crock et al., 1999). It was assumed that no other significant forms of S were present in kimberlite and processed kimberlite samples, and

Table 1
Average water compositions from the four types of waters collected for this study

| | Processed fines porewater (<i>N</i> = 60) | Process plant discharge (<i>N</i> = 9) | Upstream side of Dyke B (<i>N</i> = 9) | Upstream side of Dyke C (<i>N</i> = 9) |
|-------------------------|---|--|--|--|
| Temp (°C) | 11.89 (3.01) | 14.78 (5.07) | 12.16 (2.19) | 12.39 (2.27) |
| pH | 7.38 (0.52) | 8.38 (0.61) | 7.96 (0.69) | 7.42 (0.51) |
| SO ₄ | 1597 (1243) | 212 (167) | 128 (56) | 92 (43) |
| Mg | 328.9 (257.8) | 49.8 (27.5) | 33.2 (15.8) | 25.9 (10.7) |
| Ca | 191.0 (145.5) | 25.7 (18.3) | 20.1 (9.6) | 17.6 (5.8) |
| Alkalinity ^a | 57.3 (21.5) | 64.2 (10.6) | 57.2 (23.5) | 38.8 (17.9) |
| K | 27.3 (12.2) | 64.1 (19.7) | 24.2 (8.9) | 20.4 (11.3) |
| Na | 13.4 (6.4) | 15.3 (4.7) | 7.5 (3.4) | 9.1 (3.8) |
| Cl | 5.3 (1.0) | 30.8 (16.3) | 11.2 (5.8) | 25.4 (17.4) |
| Si | 5.90 (1.54) | 4.36 (0.66) | 1.60 (0.60) | 1.53 (0.63) |
| Ag | 0.0008 (0.0008) | 0.0002 (0.0001) | 0.0001 (0) | 0.0001 (0) |
| Al | 0.0182 (0.0290) | 0.0010 (0.0008) | 0.0049 (0.0026) | 0.0046 (0.0015) |
| As | 0.0058 (0.0019) | 0.0126 (0.0041) | 0.0059 (0.0034) | 0.0039 (0.0021) |
| B | 0.0214 (0.0108) | 0.0528 (0.0227) | 0.0234 (0.0059) | 0.0211 (0.0096) |
| Ba | 0.032 (0.017) | 0.316 (0.230) | 0.116 (0.019) | 0.149 (0.015) |
| Cd | 0.00131 (0.00073) | 0.00066 (0.00032) | 0.00043 (0.00036) | 0.00038 (0.00037) |
| Co | 0.00138 (0.00096) | 0.00051 (0.00019) | 0.00028 (0.00018) | 0.00019 (0.00011) |
| Cr | 0.00096 (0.00102) | 0.00258 (0.00317) | 0.00346 (0.00375) | 0.00209 (0.00223) |
| Cu | 0.00391 (0.00224) | 0.00156 (0.00094) | 0.00209 (0.00183) | 0.00172 (0.00112) |
| Fe | 0.530 (0.640) | 0.046 (0.050) | 0.068 (0.073) | 0.047 (0.059) |
| Mn | 0.0754 (0.0526) | 0.0161 (0.0119) | 0.0093 (0.0086) | 0.0065 (0.0052) |
| Mo | 0.771 (0.339) | 0.409 (0.116) | 0.223 (0.117) | 0.158 (0.086) |
| Ni | 0.154 (0.117) | 0.055 (0.073) | 0.021 (0.009) | 0.016 (0.007) |
| Pb | 0.00017 (0.00013) | 0.00006 (0.00012) | 0.00009 (0.00007) | 0.00007 (0.00003) |
| Sb | 0.00473 (0.00107) | 0.02793 (0.00823) | 0.00967 (0.00654) | 0.00951 (0.00462) |
| Se | 0.00398 (0.00465) | 0.00258 (0.00101) | 0.00099 (0.00080) | 0.00093 (0.00045) |
| Sr | 2.48 (1.85) | 0.52 (0.29) | 0.33 (0.14) | 0.29 (0.11) |
| U | 0.00076 (0.00066) | 0.00020 (0.00016) | 0.00027 (0.00020) | 0.00031 (0.00014) |
| V | 0.0153 (0.0304) | 0.0039 (0.0020) | 0.0015 (0.0004) | 0.0010 (0.0004) |
| Zn | 0.0175 (0.0157) | 0.0042 (0.0037) | 0.0020 (0.0015) | 0.0025 (0.0017) |
| NH ₃ -N | 0.788 (0.768) | 1.121 (0.430) | 0.186 (0.247) | 0.210 (0.164) |
| F | 0.103 (0.059) | 0.076 (0.005) | 0.070 (0.017) | 0.070 (0.026) |
| NO ₃ -N | 7.22 (18.9) | 5.24 (3.43) | 2.03 (1.63) | 3.81 (0.87) |
| NO ₂ -N | 0.222 (0.570) | 0.201 (0.133) | 0.380 (0.429) | 0.263 (0.318) |
| PO ₄ -P | 0.0149 (0.0082) | 0.0250 (0.0279) | 0.0056 (0.0051) | 0.0042 (0.0046) |
| DOC | 8.71 (5.13) | 6.20 (5.25) | 9.38 (7.57) | 7.51 (6.00) |
| DO ₂ | 6.0 (3.1) | 8.2 (1.0) | 10.4 (0.9) | 10.0 (0.7) |

Bracketed values indicate the standard deviation for each parameter. All parameters reported to be below detection were assigned the detection limit value for statistical calculations.

^a Alkalinity reported as mg/l CaCO₃.

sulphide-S was determined as the difference between these two values. Inorganic C concentration in the suite of samples was determined using coulometric titration.

X-ray diffraction analyses were conducted on the clay-sized fraction (<5 µm) of the LLCF processed kimberlite fines. The method used to separate the <5 µm size fraction is based on Stoke's Law for the settling rate of particles in a fluid. This size fraction was separated by washing the >0.6 mm size fraction of processed fines with distilled water while using an ultrasonic gun to dislodge fine-grained

material from the surface of larger grains. The resulting suspension was centrifuged for approximately 20 s at 1000 rpm. This step was used to cause all material that was >5 µm to settle out, leaving particles <5 µm in suspension. Next, the suspension was centrifuged again for 60 s at 6000 rpm, causing all material to settle out of suspension. The supernatant was decanted and the residue was poured onto a glass slide and allowed to dry subsequent to X-ray diffraction analysis, which was conducted and interpreted using the techniques described by Brindley (1980).

5. Results and discussion

The main objectives of this research were to: (a) geochemically and mineralogically describe the water-rock system in the LLCF; and, (b) to elucidate the processes that were controlling the chemistry of waters found in the LLCF.

5.1. Water chemistry

Table 1 lists analyses of the four kinds of water samples collected for this investigation. Average pore-water, discharge water, and surface water values from 2000 to 2002 are listed in this table together with standard deviation values (in parentheses). These data demonstrate that all water samples collected from the LLCF are dominated by dissolved SO₄, Mg, Ca, K, Na, HCO₃, Cl, and Si. Similar to water samples collected from the coarse kimberlite reject material described by Day et al. (2003), LLCF processed fines pore-water pH values are approximately neutral, total Fe concentrations are very low, and trace metal concentrations are generally low.

Fig. 3 is a Piper diagram, which plots, both separately and collectively, the relative content of the major cations and anions in the four types of water samples collected from the LLCF. While both the cation and anion ternary plots in Fig. 3 indicate that the four types of LLCF water samples contain differing relative cation and anion compositions, the most significant chemical distinctions between water types can be drawn from the cation ternary. This diagram demonstrates that the LLCF water samples fall into three main chemical types, based on their relative cation content. The first type, composed solely of pore-water samples, is characterized by relative cation proportions of approximately 55–80% Mg, 20–30% Ca, and up to 20% Na + K. The second water type found within the LLCF, composed solely of process plant discharge water samples, is characterized by approximately 40–65% Mg, 10–20% Ca, and 20–50% Na + K. The third distinct chemical type found in the suite of LLCF waters collected for this investigation, composed solely of surface waters collected from both the upside of Dyke B and Dyke C, is characterized by a relative cation distribution of approximately 30–55% Mg,

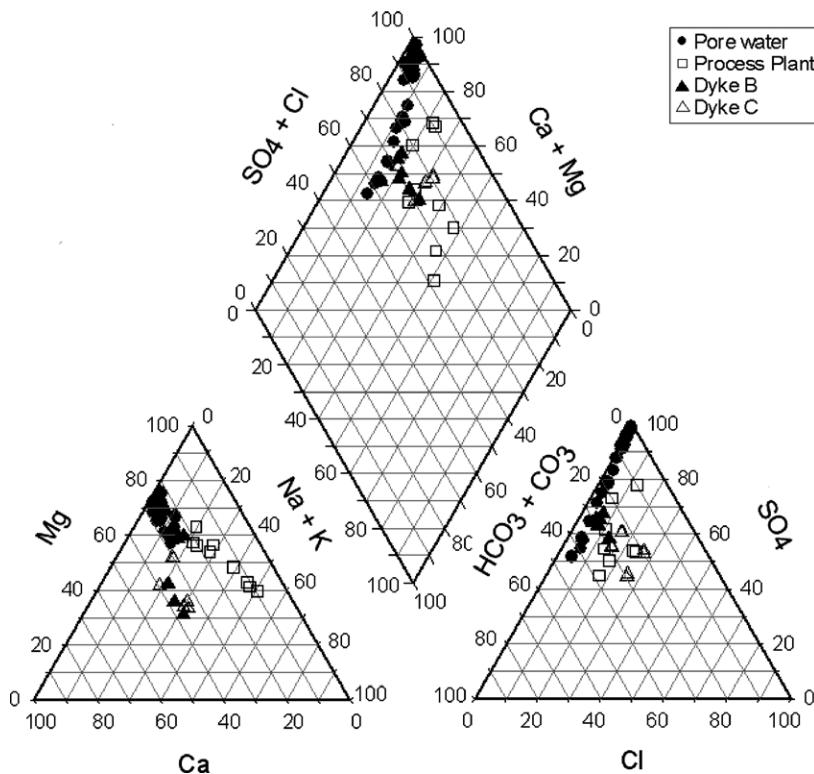


Fig. 3. Piper diagram for water samples collected from 2000 to 2002.

30–40% Ca, and 15–35% Na + K. It is important to note that while there is overlap in the absolute solute concentrations of the four types of LLCF water samples, as indicated in Table 1, Fig. 3 indicates that there is a significant difference between the chemical signature of the three water types identified, showing that water-rock reactions are taking place.

Pore-water, discharge water, and surface water samples were collected over three field seasons in order to evaluate annual variation, with two sample suites collected during the final field season; one at the beginning of the summer and one at the end of the summer, in order to evaluate seasonal changes in solute concentrations. Results indicate that while there is little seasonal change in solute concentrations in pore-water or Dyke B surface water samples, there is a steady increase in Dyke C surface water concentrations, most likely a result of the constant input of process plant discharge water to Cell C during this investigation (Fig. 4).

The concentrations of most of the solutes in processed kimberlite fines pore-water samples do not exhibit any strong increasing or decreasing trends over the 3a. Exceptions include decreases in Fe, Cr and NH_3 and increases in H^+ and B over time.

5.2. Kimberlite ore and processed kimberlite fines

Kimberlite ore and processed fines examined for this study originated from the upper portions of the Panda pipe, which is dominated by volcanoclastic kimberlite with lenses and blocks of epiclastic sediments throughout. More than 70% of the rock consists of serpentine and forsteritic olivine, with lesser spinel, pyroxene, garnet, phlogopite, pyrite, calcite and smectite.

Mud xenoclasts are present throughout the Panda kimberlite as clasts ranging in size from several mm to several cm. In hand specimen the mud-clasts are uniformly fine-grained, dark grey to black in colour, and in thin section, the mudstone is medium to dark brown and opaque (Fig. 5). X-ray diffraction analysis of the mud xenoclast indicates that smectite, quartz, and pyrite are the main minerals present in this material. Due to the similarity in appearance of the kimberlite groundmass material and the mud xenoclasts, it is difficult to discern how much of the mudstone has been incorporated into the kimberlite, which is in agreement with previous studies indicating that much of the volcanoclastic kimberlite from the Lac de Gras area

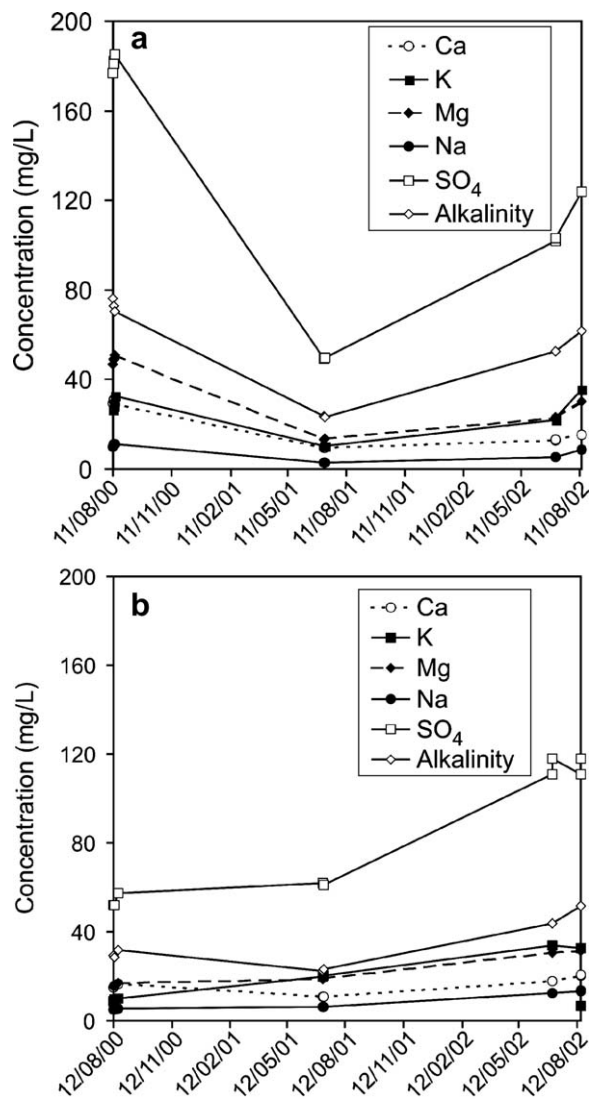


Fig. 4. Temporal behaviour of major solutes from (a) Dyke B and (b) Dyke C.

contains mud-rich inter-clast matrices (Field and Scott-Smith, 1998; Graham et al., 1998).

Sulphide minerals are restricted to the mud xenoclasts in the Panda kimberlite. The very fine framboidal grains of pyrite observed in the mudstone xenoclasts in unprocessed ore range in size from approximately 0.5–10 μm in diameter, with the majority less than 5 μm in diameter. The framboidal habit of these pyrite grains is indicative of precipitation by SO_4 -reducing bacteria in marine sediments, which is consistent with the presence of marine dinoflagellate and fish fossils found within mudstone clasts from the Lac de Gras region, suggesting that the Western Interior Seaway extended over the

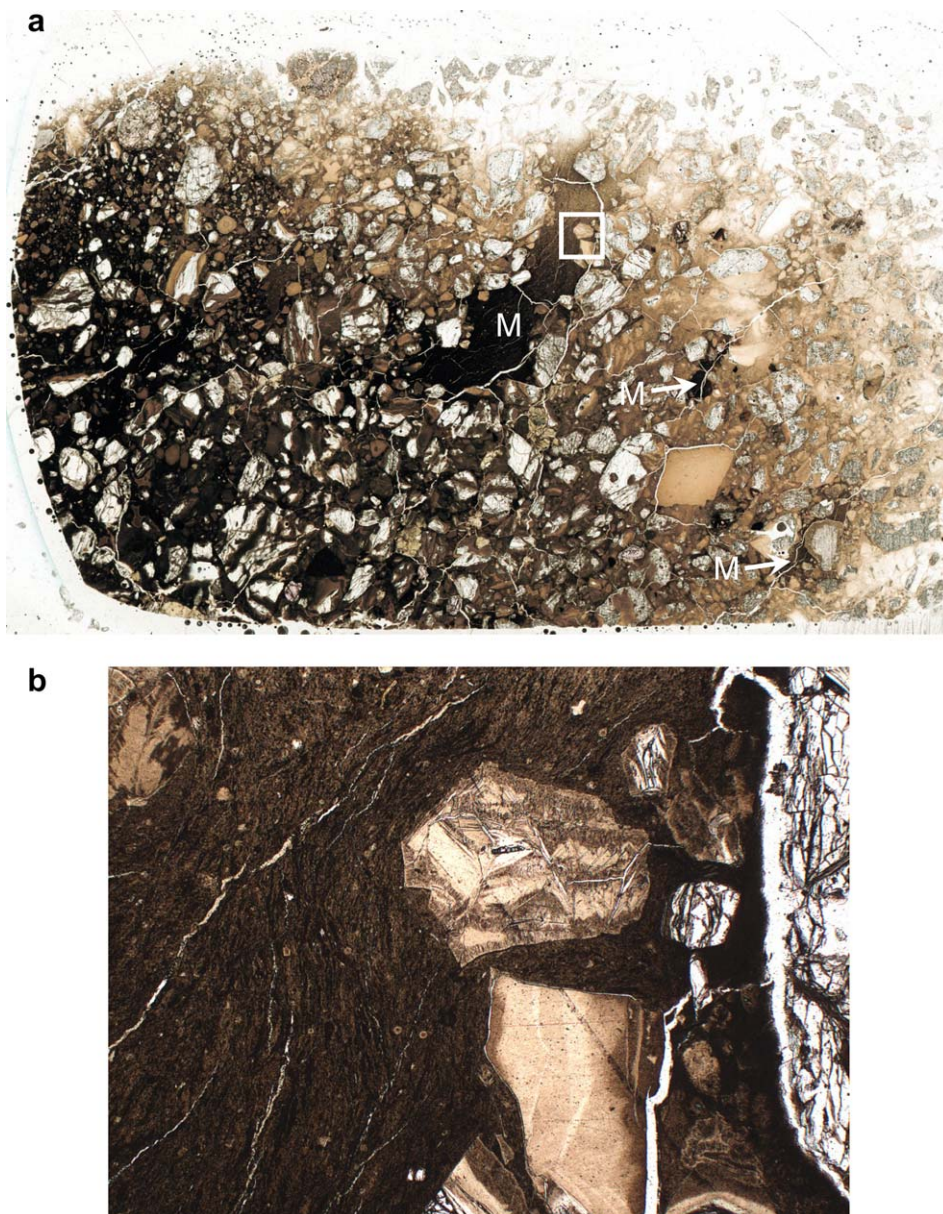


Fig. 5. (a) Panda kimberlite polished thin section indicating the location of mud xenoclasts (M). Note the variable size and shape, and fine-grained nature of these clasts and the similarity in appearance of the mud and kimberlite matrix on the left side of the image. Also note the olivine and serpentine grains embedded into the margins of mud xenoclasts (FOV = 34 mm \times 22 mm). (b) Magnified view of area indicated by the white box in (a). Note the deflection of the planar fabric of the mud xenoclasts around the embedded grains suggesting pre-lithification incorporation of the mud into the kimberlite (FOV = 2 mm \times 1.34 mm).

Slave, for at least a short time, during the Upper Cretaceous (Doyle et al., 1998; Field and Scott-Smith, 1998; Nassichuk and Dyke, 1998; Nassichuk and McIntyre, 1995; Nowicki et al., 2003).

Sulphate minerals were not easily identified in the kimberlite ore by optical means. However, X-ray element mapping and EDS spectra indicate the presence of a Ca- and S-rich phase within the mud xen-

oclasts, most likely a Ca sulphate (Figs. 6 and 7). These maps show that Ca sulphate is found as fine-grained disseminations, as well as fracture filling precipitates within the clasts.

The Panda kimberlite also contains ancient wood fragments, present as pieces up to 1 m in length, dispersed throughout the pipe. The wood, which is similar to the redwoods *Sequoia* and *Metasequoia*,

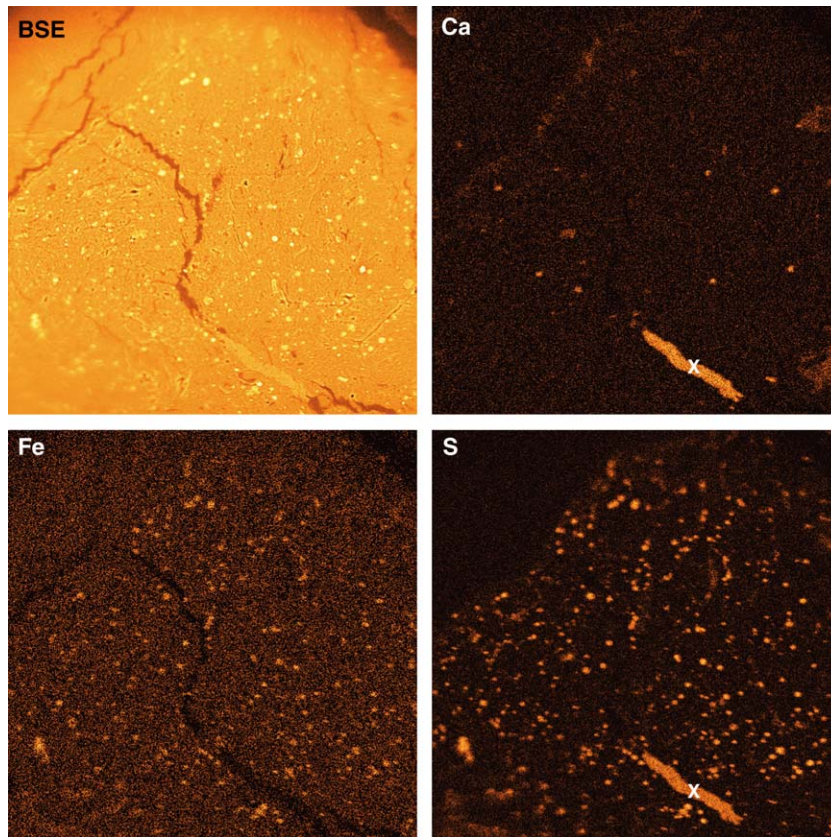


Fig. 6. Backscattered electron image of mud xenoclast from Panda kimberlite accompanied by Ca, Fe, and S X-ray element maps of the same region. Small Fe sulphide grains and a larger fraction filling of Ca sulphate are shown. Operating conditions: 15 kV accelerating voltage, 125 nA beam current, 200 times magnification, 1000 passes. The 'x' noted on the Ca and S maps note the position of the EDS spectrum shown in Fig. 7.

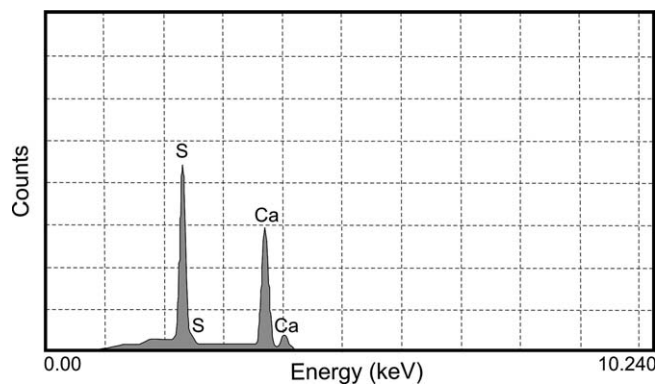


Fig. 7. Energy dispersive spectra collected from the location marked 'x' in Fig. 6.

appears relatively fresh and unaltered with marginal amounts of permineralization (Nassichuk and Dyke, 1998; Nassichuk and McIntyre, 1995).

The processed kimberlite fines are medium green-grey with no observable reaction fronts or Fe oxide

staining, and have mineralogy similar to the kimberlite ore discussed previously. Saponite, chrysotile and phlogopite were identified in the clay fraction by XRD. Similar to the kimberlite ore, pyrite in the fines is found only within mudstone fragments

and is present as framboidal grains ranging in size from approximately 0.5–10 µm in diameter, with the majority less than 5 µm in diameter. These pyrite grains maintain their framboidal habit and do not exhibit any evidence of oxidation, such as rims or Fe oxide staining around the grains.

During dry periods in the summer, a fine-grained white efflorescent crust forms on the surface of the processed kimberlite fines. As soon as it rains, this efflorescent precipitate immediately dissolves. X-ray diffraction analysis of this material indicates that it is predominantly hexahydrate ($\text{MgSO}_4 \cdot 6\text{H}_2\text{O}$).

As seen in Table 2, inorganic-C is higher in fines relative to the ore, $\text{SO}_4\text{-S}$ is concentrated in the mud, and almost absent from the fines, and sulphide-S is concentrated in the mud xenoclast, and does not change from ore to fines. The relatively large increase in inorganic-C content in the fines relative to the ore indicates that carbonate minerals most likely have precipitated in the processed kimberlite fines at some point after mining of the ore. The pattern of $\text{SO}_4\text{-S}$ concentrations is exactly opposite to that of inorganic C with the highest concentrations of $\text{SO}_4\text{-S}$ in the mud xenoclasts and the

lowest concentrations in the processed kimberlite fines, indicating that mud xenoclasts are the main source of sulphate minerals in the kimberlite ore and that SO_4 is being removed from the processed kimberlite at some point after the ore is extracted from the open pit. Similar to $\text{SO}_4\text{-S}$, sulphide-S is most concentrated in the mud xenoclasts. The difference in sulphide-S between the ore and the fines is insignificant, which is consistent with the observed fine-grained, apparently unoxidized pyrite and Ca sulphate in the mud, and suggests that dissolved SO_4 originates mostly from sulphate minerals found in mudstone material.

5.3. Controls on water chemistry

Saturation indices calculated using PHREEQC (Parkhurst and Appelo, 1999) and the Lawrence Livermore National Laboratory database included with the software indicate that chrysotile, forsterite, enstatite, diopside, and gypsum (representing Ca sulphate), all of which are minerals found in the Panda Kimberlite, are undersaturated in all waters from the containment facility (Table 3). This suggests that dissolution of all or some of these miner-

Table 2
Inorganic- CO_2 , sulphate-S, and sulphide-S analyses of mud xenoclasts, kimberlite ore, and processed kimberlite fines

| Sample type | Inorganic- CO_2 (wt%) | | | Sulphate-S (wt%) | | | Sulphide-S (wt%) | | |
|-----------------------|--------------------------------|------|-----------------|------------------|------|-----------------|------------------|------|-----------------|
| | P ₅ | Mean | P ₉₅ | P ₅ | Mean | P ₉₅ | P ₅ | Mean | P ₉₅ |
| Mud xenoclast (6) | 0.40 | 0.50 | 0.68 | 0.18 | 0.27 | 0.38 | 1.82 | 2.54 | 3.19 |
| Kimberlite ore (3) | 1.10 | 1.40 | 1.91 | 0.12 | 0.14 | 0.16 | 0.20 | 0.21 | 0.22 |
| Kimberlite fines (17) | 1.38 | 2.38 | 3.04 | 0.01 | 0.04 | 0.09 | 0.17 | 0.25 | 0.35 |

P₅ and P₉₅ represent the 5th and 95th percentile values. Bracketed numbers indicate the number of samples analyzed.

Table 3
Mean saturation indices from LLCF water samples

| | Formula | Pore-water | Discharge | Dyke B | Dyke C |
|------------------------|---|------------|-----------|--------|--------|
| Chrysotile | $\text{Mg}_2\text{Si}_2\text{O}_5(\text{OH})_4$ | -1.42 | -0.57 | -0.21 | -5.99 |
| Forsterite | Mg_2SiO_4 | -7.31 | -6.50 | -6.26 | -10.12 |
| Enstatite | MgSiO_3 | -2.72 | -2.46 | -2.51 | -4.45 |
| Diopside | $\text{CaMgSi}_2\text{O}_6$ | -3.93 | -3.59 | -3.53 | -7.41 |
| Goethite | FeOOH | 5.38 | 4.90 | 4.70 | 4.38 |
| Gypsum | CaSO_4 | -0.78 | -1.94 | -2.14 | -2.32 |
| Montmorillonite | | ~5.0 | ~2.6 | ~1.4 | ~1.5 |
| Saponite | | ~3.8 | ~3.5 | ~2.6 | ~-3.3 |
| Calcite | CaCO_3 | -0.17 | -0.05 | -0.19 | -1.02 |
| Amorph. SiO_2 | SiO_2 | -0.79 | -1.00 | -1.39 | -1.43 |
| Brucite | $\text{Mg}(\text{OH})_2$ | -3.94 | -3.18 | -3.42 | -4.78 |
| Magnesite | MgCO_3 | -0.35 | -0.10 | -0.36 | -1.25 |
| Sepiolite | $\text{Mg}_4\text{Si}_6\text{O}_{15} \cdot 6\text{H}_2\text{O}$ | -1.98 | -1.77 | -2.44 | -10.22 |
| $\text{CO}_{2(g)}$ | CO_2 | -3.30 | -3.59 | -3.73 | -3.23 |

als produces the Mg–Ca–SO₄ character of the discharge and pore waters. Montmorillonite and saponite are consistently oversaturated in all LLCF waters, calcite is undersaturated in pore- and surface water samples and near saturation in discharge water samples, and silica is close to saturation in pore-water samples but undersaturated in discharge and surface water samples. As well, it should be noted that Fe(OH)₃ is slightly supersaturated in the pore-water samples.

5.3.1. Pore-water

The ephemeral efflorescent Mg sulphate on the surface of the processed kimberlite fines suggests that evaporation may be an important factor affecting pore-water composition. Sulphate has been chosen as a conservative tracer due to the fact that it is present in a wide range of concentrations and is not seen to precipitate from solution until very high salinities are reached. Analysis of data from the suite of pore-water samples collected for this study indicates that, in addition to SO₄, Ca and Mg (the most abundant cations) remain concentrated in solution as evaporation progresses (Fig. 8a,b). These data suggest that no minerals containing these elements are precipitating from the pore-waters sampled (with the exception of the Mg sulphate forming occasionally from extreme evaporation of near-surface solutions, as described above) and that the behaviour of these elements in solution is largely controlled by evaporation. However, silica and HCO₃ concentrations are relatively constant at all degrees of evaporation (Fig. 8c,d), suggesting that there is some mechanism controlling the concentration of each of these two dissolved constituents. In addition, Na and K plot in a linear trend below the calculated evaporation field suggesting that these two elements are being progressively removed from solution during evaporation (Fig. 8e,f).

Aqueous stability diagrams have been constructed in order to investigate the minerals and reactions that might be controlling the chemistry of a given solution. All phase diagrams were constructed using the dissolution reactions and equilibrium constants found in the Lawrence Livermore National Laboratory thermodynamic database distributed with the PHREEQC software. A projection of the LLCF water sample compositions on the MgO–SiO₂–Al₂O₃–H₂O phase diagram (Fig. 9) indicates that amorphous silica is controlling the silica content of LLCF waters. The average P_{CO_2} for

LLCF samples, as determined from CO_{2(g)} SI values (Table 3), is relatively constant with values ranging from 10^{-3.73} atm up to 10^{-3.23} atm. As well, the SI values for calcite and magnesite in Table 3 suggest that calcite and magnesite are undersaturated in the pore and surface water samples. However, it should be noted that the discharge water has calcite and magnesite SI values close to 0. These data suggest that alkalinity in the LLCF is currently being controlled by ambient atmospheric CO₂ concentrations. The mechanism removing Na and K from solution could be the result of a combination of mechanisms including clay mineral precipitation, ion exchange, surface adsorption, and biogenic action (Eugster and Jones, 1979). Note that for most water samples, saponite and kaolinite are indicated to be stable, but not necessarily precipitating.

In most examples of evaporation, Cl is chosen as the conservative tracer since it forms highly soluble salts and is present in solution until the very latest stages of evaporation. However, Cl in pore-water samples from EKATI maintains a relatively constant concentration, ranging from 3 mg/l up to a maximum of 7.5 mg/l (Table 1), and no Cl-bearing phases were identified to be supersaturated in pore-water samples. It has been noted that kimberlite readily absorbs PO₄ and As (Graham, 2002), both of which act as hydrolyzed anions in solution. Craw (2000) suggested that Cl⁻ ions, as well as alkali ions, could be adsorbed to phyllosilicates as part of the progressive groundwater alteration of schist. The absorptive ability of kimberlite material could help to explain the relatively constant Cl concentrations observed within the fines pore-water, but further work is required to more fully explain this phenomenon.

While the causes of the Cr and B concentration variations in pore waters are unknown, it is likely that the increase in H⁺ (decreasing pH) is, in part, a result of the oxidation of NH₃ from remnant blasting residue, forming NO₃. This decrease in the pH of pore waters is probably not the result of sulphide oxidation, since SO₄ is not observed to increase over time.

5.3.2. Surface water

The temporal changes in the surface water at Dyke B appear to be directly related to changing water levels and dilution, most significantly by snow melt runoff which ponded in the south end of Cell B. Water levels immediately North of Dyke B were sig-

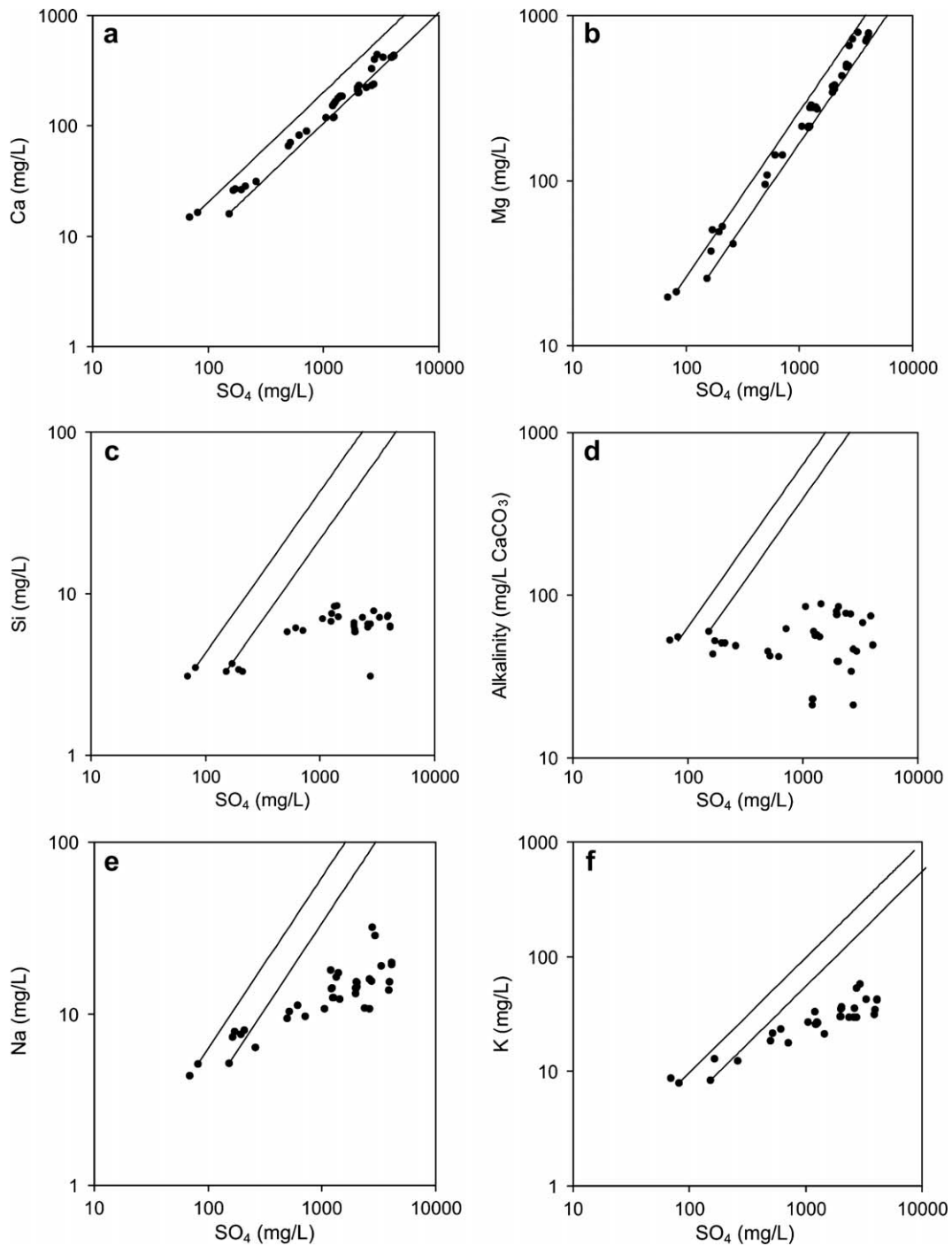


Fig. 8. Plots showing the behaviour of (a) Mg, (b) Ca, (c) Si, (d) alkalinity, (e) Na, and (f) K during evaporation of the LLCF processed kimberlite pore-water. The two solid lines bracket the range of concentrations that can be expected through evapoconcentration of the most dilute pore-water samples.

nificantly higher in 2001 than either 2000 or 2002, which coincided with a marked decrease in solute concentrations in Dyke B water samples during this time (Fig. 4a). These data suggest that solute behav-

our at Dyke B during this investigation was controlled by dilution.

Similar to the results from seasonal sampling, the increasing annual trend of all solutes at Dyke C

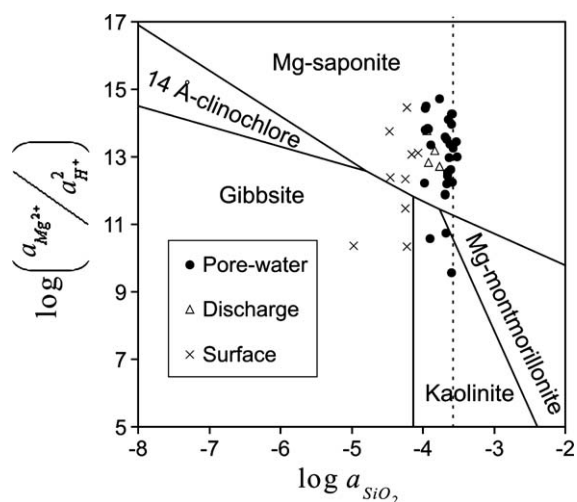


Fig. 9. Mineral stability diagram for the MgO–SiO₂–Al₂O₃–H₂O system constructed at 12 °C. Note that Al is assumed to be conservative in this diagram.

appears to be directly influenced by the discharge of process plant water to Cell C (Fig. 4b).

5.3.3. Process plant discharge water

The reactions that occur through the mineral processing circuit directly affect the composition of waters in the containment facility. Inverse modeling has been used, together with representative water analyses and Panda kimberlite mineralogy, to calculate phase transfers that could be responsible for the water chemistry being discharged from the process plant during the crushing and washing of Panda ore. The majority of water that entered the containment facility during this investigation was taken from the north side of Dyke C and was used in the processing of kimberlite ore before it was discharged to the LLCF. Therefore, Dyke C and process plant discharge water samples exist along the same flow path through the process plant.

Although numerous models of calculated mass transfers are mathematically possible, geochemically reasonable scenarios were selected based on knowledge of the minerals involved and their stability under the conditions present in the processing plant (Hudson-Edwards et al., 2005). Table 4 lists the process plant discharge and Dyke C water analyses that were used to perform inverse modeling calculations. Only major elements were used for inverse modeling because they make up more than 90% of the water analyses, on an equivalent basis, and their abbreviation does not significantly affect charge balance of these solutions. Chloride was

Table 4
Dyke C surface water and process plant discharge water analyses used in inverse modeling calculations

| | Dyke C | Discharge |
|--------------------------------------|-----------|-----------|
| Sample Date | 04-Jul-02 | 09-Jul-02 |
| Temperature (°C) | 16.35 | 20.25 |
| pH | 8.08 | 7.74 |
| DO | 9.99 | 7.84 |
| Alkalinity (mg/L CaCO ₃) | 43.6 | 59.6 |
| Ca | 17.8 | 54.1 |
| Fe | 0.005 | 0.018 |
| K | 33.7 | 81.2 |
| Mg | 30.5 | 90.2 |
| Na | 12.3 | 22.5 |
| Si | 2.00 | 4.9 |
| Cl | 43 | 55 |
| SO ₄ | 118 | 472 |

included since its concentrations increase noticeably through the mineral processing circuit, and Fe was included to investigate the role of sulphide oxidation. The phases included in the mass-balance calculations (Table 5) were chosen based on the mineralogical work discussed previously. Although no significant concentrations of Cl-bearing minerals were found in the kimberlite ore, halite was added to the list of phases to represent a source of Cl (Eary et al., 2003; Hudson-Edwards et al., 2005).

Four separate scenarios were modeled. The first scenario assumed that gypsum is the main source of SO₄ and that the increase in Fe through the process plant is negligible. Therefore, Fe was omitted from the solution chemistry as well from the phases used in these calculations. Scenario two was similar to scenario one, except fayalite was included as a source of Fe. This scenario was intended to determine the amount of fayalite required to produce the change in dissolved Fe concentrations observed. The third scenario included both gypsum and pyrite as potential sources of SO₄. Pyrite was included in this scenario to determine the amount required to account for the increase in dissolved Fe. Finally, scenario 4 represented the end-member situation in which all the dissolved SO₄ is due to pyrite oxidation alone. However, all models generated using this scenario require the precipitation of a large amount of chrysotile, a result that is unlikely since chrysotile is undersaturated in the discharge water. Such a process is also unlikely for kinetic reasons. Therefore, no models generated using scenario 4 were considered geochemically feasible. Table 5 depicts the three most reasonable sets of mole transfers produced from these models. All calculations were

Table 5
Mass transfer models calculated using PHREEQC

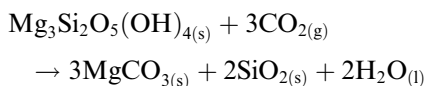
| Mineral | Formula | 1 | 2 | 3 |
|---------------------|---|------------|--------------|-------------|
| Magnesite | MgCO ₃ | -17.88 | -17.86 | -17.63 |
| Chrysotile | Mg ₃ Si ₂ O ₅ (OH) ₄ | 5.959 | 5.954 | 5.875 |
| CO ₂ (g) | CO ₂ | 17.88 | 17.86 | 17.63 |
| Forsterite | Mg ₂ SiO ₄ | - | - | - |
| Gypsum | CaSO ₄ · 2H ₂ O | 0.003954 | 0.004151 | 0.004147 |
| Halite | NaCl | 0.0006 | 0.0005957 | 0.0005922 |
| Saponite-Ca | Ca _{0.165} Mg ₃ Al _{0.33} Si _{3.67} O ₁₀ (OH) ₂ | -0.01789 | -0.01908 | -0.01907 |
| Saponite-K | K _{0.33} Mg ₃ Al _{0.33} Si _{3.67} O ₁₀ (OH) ₂ | 0.003012 | 0.004247 | 0.004239 |
| Saponite-Mg | Mg _{3.165} Al _{0.33} Si _{3.67} O ₁₀ (OH) ₂ | 0.01500 | 0.01495 | 0.01493 |
| Saponite-Na | Na _{0.33} Mg ₃ Al _{0.33} Si _{3.67} O ₁₀ (OH) ₂ | -0.0001234 | -0.0001106 | -0.0001048 |
| Am. Silica | SiO ₂ | -11.92 | -11.91 | -11.75 |
| Fayalite | Fe ₂ SiO ₄ | NI | 0.0000001261 | NI |
| Pyrite | FeS ₂ | NI | NI | 0.000000252 |

The three sets of inverse calculations correspond to scenarios described in the text. All mole transfers are reported in terms of moles of phase transferred per kilogram of solution. Positive mole transfers indicate dissolution and negative mole transfers indicate precipitation. Note that dashes indicate that the phase was not indicated to dissolve or precipitate by the model and NI indicates that the phase was not included in modeling calculations.

repeated using calcite instead of magnesite as the carbonate mineral, which produced very small differences in mole transfers (e.g. mole transfer of gypsum increased from 0.003954 to 0.004195) compared to those in Table 5 (Rollo, 2003).

Table 5 indicates that the main mole transfers in all geochemically feasible models are the dissolution of chrysotile and CO₂(g), and the precipitation of amorphous silica and a carbonate mineral. While the carbonate listed in Table 5 is magnesite, essentially identical quantities of calcite would be precipitated if that was the chosen carbonate mineral. A small amount of gypsum is shown to dissolve in all cases. The net mole transfer of saponite in all models is essentially zero. Fig. 9 indicates that saponite is stable in LLCF waters. Therefore, the mass-transfer of the various saponite minerals to and from solution can be considered in terms of sorption and cation exchange reactions between clay minerals in the kimberlite. Note that all models that included Fe involved very small mole transfers of the Fe-bearing phase and did not significantly affect the mole transfers of other phases.

These data suggest that the net reaction occurring during the processing of kimberlite ore is:



The proposed reaction, shown above, involves the dissolution of chrysotile and CO₂ in the process plant water and the precipitation of magnesite and amorphous silica. This is consistent with the fact that the inorganic C content increases from ore to

finer (Table 2), and the calculated SI value of silica and carbonate minerals are near saturation in discharge waters (Table 3). This is the same reaction proposed for most mineral carbonation schemes (e.g. Lackner, 2002), and suggests that crushed kimberlite may provide a potential option for safe sequestration of anthropogenic C emissions. Cipolli et al. (2004) have used reaction path modeling to demonstrate that CO₂ injection into serpentinite reservoirs would sequester a significant amount of CO₂ within several decades. Hansen et al. (2005) have suggested that the mineral transformation that produced carbonate-altered serpentinite at Atlin, British Columbia, is a natural analogue to proposed CO₂ sequestration processes.

The modeling results suggest that CO₂ sequestration is actively occurring in the kimberlite processing plant. As kimberlite ore is crushed and washed, CO₂ from the atmosphere appears to dissolve in the process water producing protons. These protons, together with dissolved carbonate, then react with chrysotile to form magnesite and silica. Further work is focusing on whether mineral carbonation using serpentine-rich kimberlite can be used to reduce CO₂ emissions at the diamond mine.

Discharge water is undersaturated with respect to gypsum indicating that, if present, gypsum will dissolve. The kimberlite ore contains an average SO₄-S concentration of 0.14% (Table 2) while the processed kimberlite fines contain essentially no SO₄-S, suggesting that the small amount of SO₄ in the ore dissolved during processing. The mass-balance calculations presented in Table 5 are consistent with

these observations since the models indicate that the dissolution of a small amount of gypsum accounts for the increase in SO_4 concentrations observed through the processing plant circuit.

6. Conclusions

Analysis of water samples indicate that all waters from the LLCF are dominated by SO_4 , Ca, Mg, Na, K, and HCO_3 . In addition, these samples have circumneutral pH values and low total dissolved Fe. Both the kimberlite ore and the processed kimberlite fines are similar in mineralogy, consisting predominantly of chrysotile and forsterite. Both sulphide and sulphate minerals were identified and found only in mudstone xenoclasts. All the dissolved SO_4 appears to have originated from the kimberlite ore, but the sulphides do not show any signs of oxidation, either macroscopically or microscopically. In addition, there is no Fe oxide staining in the LLCF.

The results of the investigation suggest that the Ca sulphate present in the mud xenoclasts, although volumetrically minor, is the origin of the relatively high dissolved SO_4 and at least some of the Ca in the discharge and pore waters. High dissolved Mg originates from the dissolution of chrysotile, the volumetrically dominant mineral in the ore. Pyrite dissolution, which is not apparent in thin section, is relatively unimportant at this stage of the chemical evolution of these waters. Eventually the pyrite may oxidize in those fines in the active layer that are briefly unfrozen during the short Arctic summer. The implication for diamond mine operators in the Lac de Gras kimberlite field is that the amount of dissolved SO_4 in mine waste water is directly related to the amount of mud xenoclasts present, as these materials host both the sulphate and sulphide minerals.

The study also indicates that the composition of the water in the LLCF is primarily the result of water-rock interactions occurring within the processing plant. Dissolution of Mg silicates and Ca sulphate occurs very rapidly as the ore spends approximately 1 h in the processing plant. [Craw \(2000\)](#) has shown that water interacting with fresh excavated greenschist facies schist acquires a distinctive composition indicative of water-rock reaction including chlorite dissolution very rapidly, on the scale of weeks or months. At EKATI, once the processed fines are deposited in the LLCF, evaporation during the short, dry Arctic summer is the dominant control on water chemistry, increasing Ca, Mg, and SO_4 concentrations. Modeling indi-

cates that amorphous silica and a carbonate mineral precipitate in the fines, although further work is necessary to confirm this. The results suggest that the water-rock interaction in the processing plant includes the dissolution of atmospheric CO_2 and mineral carbonation processes similar to those proposed for CO_2 sequestration schemes, which is supported by recent experiments in the authors' laboratory ([Lee, 2005](#)).

The Panda kimberlite is the first of 8 pipes that will be processed at EKATI diamond mine. Given that the mineralogy of the kimberlite and xenoclastic components, and the nature of water-rock interactions in the processing plant are critical in controlling effluent water composition, it is unclear whether the processes identified in this study will continue, or be replaced by others.

Acknowledgements

The authors are grateful to John Witteman and Jim Millard of EKATI diamond mine and BHPBil-liton for their support of this research. Financial support was also provided by the Natural Sciences and Engineering Research Council of Canada. Comments from David Craw and an anonymous reviewer significantly improved the manuscript.

References

- Baker, M.J., Blowes, D.W., Logsdon, M.J., Jambor, J.L., 2003. Environmental geochemistry of kimberlite materials: Diavik Diamonds Project, Lac de Gras, Northwest Territories, Canada. *Explor. Mining Geol.* 10, 155–163.
- Barnes, I., LaMarche, V.C.J., 1969. The relationship between fluids in some fresh alpine-type ultramafics and possible modern serpentinization, Western United States. *Geol. Soc. Am. Bull.* 80, 1947–1960.
- Barnes, I., LaMarche, V.C.J., Himmelberg, G., 1967. Geochemical evidence of present-day serpentinization. *Science* 156, 830–832.
- Barnes, I., O'Neil, J.R., Trescases, J.J., 1978. Present day serpentinization in New Caledonia, Oman, and Yugoslavia. *Geochim. Cosmochim. Acta* 42, 144–145.
- Borisov, V.N., Alexeev, S.V., Pleshevenkova, V.A., 1995. The diamond mining quarries of East Siberia as a factor affecting surficial water quality. In: Kharaka, Y.K., Chudaev, O.V., Thordsen, J.J., Armannsson, H., Breit, G. N., William Charles Evans, W.C., Keith, T.E.C. (Eds), 8th Internat. Symp. Water Rock Interaction, Vladivostok, Russia. A.A. Balkema, pp. 863–866.
- Brindley, G.W., 1980. Order-disorder in clay mineral structures. In: Brindley, G.W., Brown, G. (Eds.), *Crystal Structures of Clay Minerals and their X-ray Identification*. Spottiswoode Ballantyne Ltd., London, pp. 125–195.

- Bruni, J., Canepa, M., Giovanni, C., Cioni, R., Cipolli, F., Longinelli, A., Marini, L., Ottonello, G., Zuccolini, M.V., 2002. Irreversible water-rock mass transfer accompanying the generation of the neutral, Mg-HCO₃ and high-pH, Ca-OH spring waters of the Genova Province, Italy. *Appl. Geochem.* 17, 455–474.
- Carlson, J.A., Kirkley, M.B., Thomas, E.M., Hillier, W.D., 1998. Recent Canadian kimberlite discoveries. In: Gurney, J.J., Gurney, J.L., Pascoe, M.D., Richardson, S.H. (Eds.), 7th Internat. Kimberlite Conf. Red Roof Design, University of Cape Town, South Africa, pp. 81–89.
- Cipolli, G., Gambardella, B., Marini, L., Ottonello, G., Zuccolini, M.V., 2004. Geochemistry of high-pH waters from serpentinites of the Gruppo di Voltri (Genova, Italy) and reaction path modeling of CO₂ sequestration. *Appl. Geochem.* 19, 787–802.
- Craw, D., 2000. Water-rock interaction and acid neutralization in a large schist debris dam, Otago, New Zealand. *Chem. Geol.* 171, 17–32.
- Crock, J.G., Arbogast, B.F., Lamothe, J., 1999. Laboratory methods for the analysis of environmental samples. In: Plumlee G.S., Lodgson, M.J. (Eds.), *The Environmental Geochemistry of Mineral Deposits. Part A: Processes, Techniques, and Health Issues.* Society of Economic Geologists, pp. 265–287.
- Day, S., Sexsmith, K., Millard, J., 2003. Acidic drainage from calcareous coarse kimberlite reject. EKATI diamond mine, NWT, Canada. 6th Internat. Conf. Acid Rock Drainage, Cairns, Australia.
- Doyle, B.J., Kivi, K., Scott-Smith, B.H., 1998. The Tli Kwi Cho (DO27 and DO18) diamondiferous kimberlite complex, Northwest Territories, Canada. In: Gurney, J.J., Gurney, J.L., Pascoe, M.D., Richardson, S.H. (Eds.), 7th Internat. Kimberlite Conf. Red Roof Designs, University of Cape Town, pp. 194–204.
- Eary, L.E., Runnells, D.D., Esposito, K.J., 2003. Geochemical controls on ground water composition at the Cripple Creek Mining District, Cripple Creek, Colorado. *Appl. Geochem.* 18, 1–24.
- EBA Engineering Consultants Ltd., 1998. Tailings characterization study. Submitted to EKATI Environment Department.
- Eugster, H.P., Jones, B.F., 1979. Behaviour of major solutes during closed-basin brine evolution. *Am. J. Sci.* 279, 609–631.
- Field, M., Scott-Smith, B.H., 1998. Contrasting geology and near-surface emplacement of kimberlite pipes in Southern Africa and Canada. In: Gurney, J.J., Gurney, J.L., Pascoe, M.D., Richardson, S.H. (Eds.), 7th Internat. Kimberlite Conf. Red Roof Design, University of Cape Town, pp. 214–237.
- Graham, I., Burgess, J.L., Bryan, D., Ravenscroft, P.J., Thomas, E., Doyle, B.J., Hopkins, R., Armstrong, K.A., 1998. Exploration history and geology of the Diavik kimberlites, Lac de Gras, Northwest Territories, Canada. In: Gurney, J.J., Gurney, J.L., Pascoe, M.D., Richardson, S.H. (Eds.), 7th Internat. Kimberlite Conf. Red Roof Design, University of Cape Town, pp. 262–279.
- Graham, K.P., 2002. Investigation of the Fate of Wastewater Phosphorus within the Processed Kimberlite Containment Area at BHP's EKATI diamond mine, MSc thesis, Univ. Alberta.
- Hansen, L.D., Dipple, G.M., Gordon, T.M., Kellett, D.A., 2005. Carbonated serpentinite (listwanite) at Atlin, British Columbia: a geological analogue to carbon dioxide sequestration. *Can. Min.* 43, 225–239.
- Hudson-Edwards, K.A., Jamieson, H.E., Charnock, J.M., Macklin, M.G., 2005. Arsenic speciation in waters and sediment of ephemeral floodplain pools, Ríos Agrio-Guadiamar, Aznalcóllar, Spain. *Chem. Geol.* 219, 175–192.
- Kjarsgaard, B.A., Wilkinson, L., Armstrong, J.A., 2002. Geology, Lac de Gras Kimberlite Field, Central Slave Province, Northwest Territories-Nunavut; Geological Survey of Canada, Open File 3238, 1:250 000.
- Lackner, K.S., 2002. Carbonate chemistry for sequestering fossil carbon. *Ann. Rev. Energy Environ.* 27, 193–232.
- Langmuir, D.L., 1996. *Aqueous Environmental Geochemistry.* Prentice-Hall Inc., New Jersey.
- Law-West, D., 2003. *Diamonds.* Natural Resources Canada Mineral and Metals Commodity Reviews. Available from: <http://www.nrcan.gc.ca/mms/cmy/com_e.html>.
- Lee, C.A., 2005. Evaluation of the Potential Use of Processed Kimberlite to Sequester CO₂, EKATI diamond mine, NWT, Canada. MSc thesis, Queen's Univ.
- Nassichuk, W.W., Dyke, D.R., 1998. Fossils recovered from kimberlite pipes in the Lac de Gras Field, Slave Province, Northwest Canada; geological implications. 7th Internat. Kimberlite Conf., Extended Abstracts, Cape Town, pp. 612–614.
- Nassichuk, W.W., McIntyre, D.J., 1995. Cretaceous and tertiary fossils discovered in kimberlites at Lac de Gras in the Slave Province, Northwest Territories. *Geol. Surv. Canada – Curr. Res.*, 1995-B, 109–114.
- Norecol Dames and Moore, 1997. Acid/alkaline (ARD) and geochemical characterization program. Submitted to EKATI Environment Department.
- Nowicki, T.E., Carlson, J.A., Crawford, B.B., Lockhardt, G.D., Oshust, P.A., Dyck, D.R., 2003. Field guide to the EKATI diamond mine. In: Kjarsgaard, B.A. (Ed.), 7th Internat. Kimberlite Conf., Slave Province and Northern Alberta Field Trip Guidebook, pp. 39–59.
- Parkhurst, D.L., Appelo, C.A.J., 1999. *User's Guide to PHREEQC (Version 2) – A Computer Program for Speciation, Batch-Reaction, One Dimensional Transport, and Inverse Geochemical Calculations.* US Geological Survey, Denver, Colorado.
- Pfeifer, H.R., 1977. A model for fluids in metamorphosed ultramafic rocks: observations at surface and subsurface conditions (high pH spring waters). *Schweiz. Mineralog. Petrograph. Mitt.* 57, 361–396.
- Rescan Environmental Services Inc., 1996. NWT diamonds project – environmental impact statement (Vol. II). Submitted to EKATI Environment Department.
- Rollo, H.A., 2003. Processed Kimberlite-Water Interaction in Diamond Mine Waste. EKATI Diamond Mine, NWT, Canada. MSc thesis, Queen's Univ.
- Sader, J.A., Leybourne, M.I., McClenaghan, M.B., Hamilton, S.M., 2003. Geochemistry of Groundwaters from Jurassic Kimberlites in the Kirkland Lake and Lake Timiskaming Kimberlite Fields. Northeastern Ontario. *Geol. Surv. Canada Open File Report* 4515.
- Sobek, A., Schuller, W.A., Freeman, J.R., Smith, R.M., 1978. Field and laboratory methods applicable to overburdens and minesoils. Submitted to US Environmental Protection Agency – Report EPA-600/2-78-054.